

## Observation of beta-delayed proton emission from $^{24}\text{Al}$

J.C. Batchelder,\* R.J. Tighe, D.M. Moltz, T.J. Ognibene, M.W. Rowe, and Joseph Cerny

*Department of Chemistry and Lawrence Berkeley Laboratory, University of California, Berkeley, California 94720*

(Received 28 April 1994)

Utilizing the  $^{24}\text{Mg}(p, n)$  reaction and a low-energy proton detector ball, beta-delayed proton emission from  $^{24}\text{Al}$  has been observed in the form of a quasicontinuum of protons from  $\sim 300$  to  $1100$  keV. By making a comparison with a previously known  $^{24}\text{Al}$  beta-delayed alpha branching ratio, a branching ratio for beta-delayed proton emission of  $(1.2 \pm 0.3) \times 10^{-5}$  has been determined.

PACS number(s): 27.30.+t, 23.40.-s

### I. INTRODUCTION

Beta-delayed particle-decay studies have provided a wide variety of spectroscopic information. This includes information on level energies, spins, isospins, widths, densities, and beta-decay properties. There are by now well over 100 examples of delayed proton and alpha emitters. For beta-delayed emission of protons or alpha particles to occur, the beta-decay energy ( $Q_{\text{EC}}$ ) available to a potential "precursor" must exceed the proton or alpha separation energy ( $B_p$  or  $B_\alpha$ ) in its daughter, the potential "emitter." For it to compete effectively with other decay routes available to the precursor (i.e., beta-delayed  $\gamma$  decay), the energy difference  $Q_{\text{EC}} - B$  must be sufficient to allow significant beta population for at least one state in the emitter that can eject particles energetic enough to penetrate the Coulomb barrier. There have been several recent reviews on this topic [1,2].

A general trend in this research has been to study nuclei farther and farther from the valley of beta stability. However, beta-delayed particle precursors with relatively small particle branches are known to exist close to the beta stability line for light nuclei. For example, the  $A = 4n$ ,  $T_z = -1$  series of beta-delayed charged particle emitters has been observed from  $^8\text{B}$  to  $^{48}\text{Mn}$  [2]. Some of these are strictly alpha emitters, such as  $^{20}\text{Na}$ , whereas other members are only proton emitters (e.g.,  $^{48}\text{Mn}$ ). The members of this series of interest in the present work are  $^{20}\text{Na}$  and  $^{24}\text{Al}$ . Sodium-20 is a well-known delayed alpha emitter (branching ratio =  $20 \pm 2\%$  [2]). It is essentially closed to positron-delayed proton emission (the available proton decay energy is  $\sim 15$  keV), but in principle is open to electron-capture (EC) delayed proton emission (however, the ratio  $\Gamma_{\text{EC}}/\Gamma_{\beta+}$  is expected to be extremely small). Beta-delayed alpha emission from  $^{24}\text{Al}$  was first observed in 1969 [3] and has subsequently been studied in greater detail [4-6]. However, although  $^{24}\text{Al}$  is

also open to delayed proton emission ( $Q_{\text{EC}} - B_p = 2.188$ ), this decay mode has not previously been observed.

We have recently investigated low-energy beta-delayed protons emitted from the  $A = 4n + 3$ ,  $T_z = -3/2$  nucleus  $^{23}\text{Al}$ . During a 40-MeV proton bombardment of a  $^{24}\text{Mg}$  target, an apparent continuum of proton events was observed between  $\sim 300$  and  $1100$  keV. At this bombarding energy, the only potential delayed proton emitters produced in this reaction are  $^{20}\text{Na}$ ,  $^{23}\text{Al}$ , and  $^{24}\text{Al}$ . The thresholds for the  $^{24}\text{Mg}(p, \alpha n)^{20}\text{Na}$ ,  $^{24}\text{Mg}(p, 2n)^{23}\text{Al}$ , and  $^{24}\text{Mg}(p, n)^{24}\text{Al}$  reactions are 25.0, 30.8, and 15.3 MeV (laboratory proton beam energies), respectively. Consequently, to unambiguously determine the origin of the continuum of low-energy proton events observed in our  $^{23}\text{Al}$  experiments, we proceeded to perform bombardments of  $^{24}\text{Mg}$  targets with proton beams at energies of 28.5 and 20.0 MeV.

### II. EXPERIMENTAL SETUP

A helium-jet system was utilized to collect and transport reaction products to a low-background counting area. A full description of the helium-jet system is given elsewhere [7]. Briefly, our targets were located in a chamber pressurized to  $\sim 1.3$  atm with helium. Reaction products which recoiled out of the target were thermalized in the helium and were swept out of the chamber (on KCl aerosols suspended in the gas) through a 75-cm-long capillary (0.9 mm i.d.) to the counting chamber. Here they were deposited onto a tape in the center of our new low-energy proton detector ball. The tape can be moved continuously at a slow rate to reduce the beta background from longer-lived activities, but this movement makes half-life determinations extremely difficult. Therefore the tape drive system is utilized in different modes depending on the experimental requirements.

The new low-energy detector ball is capable of detecting protons with energies down to  $\sim 200$  keV. It consists of six individual gas- $\Delta E$ , gas- $\Delta E$ , Si- $E$  triple telescopes. Each telescope subtends a solid angle of approximately 4% of  $4\pi$  relative to the collection point. A full description of this detector will be given elsewhere [8]. Figure 1 depicts a cross sectional view of one such telescope. The present design uses grids rather than nickel foils (as were

\*Present address: Oak Ridge National Laboratory, Building 6008, Mail Stop 6374, Oak Ridge, TN 37831-6374.

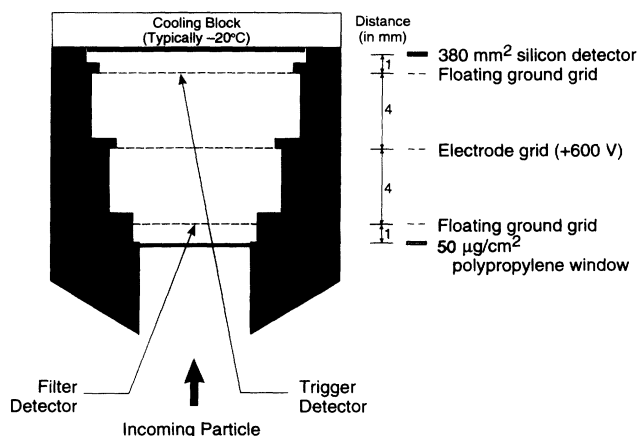


FIG. 1. Cross sectional view of one of the low-energy gas- $\Delta E$ , gas- $\Delta E$ , Si- $E$  triple telescopes.

used in a previous version [9] as electrodes. Two gas  $\Delta E$  signals (“trigger” and “filter”) are obtained from the two floating-ground grids. The gas detectors are typically pressurized to  $\sim 15$  Torr of tetrafluoromethane ( $\text{CF}_4$ ). Figure 2 schematically shows two cross sectional views of the detector ball, indicating the relative placement of the six telescopes, as well as the location of the tape drive. In helium-jet studies only four of the telescopes are used, as the collection point is obstructed by the tape drive for two of the telescopes (i.e., telescopes 5 and 6). However, each of the other four telescopes subtends the full  $\sim 4\%$  of the  $4\pi$  solid angle.

Figure 3 shows typical calibration data taken with one of these detectors from the  ${}^3\text{He} + {}^{\text{nat}}\text{Mg}$  reaction. The 40-MeV  ${}^3\text{He}$  pulsed beam was supplied by the 88-Inch

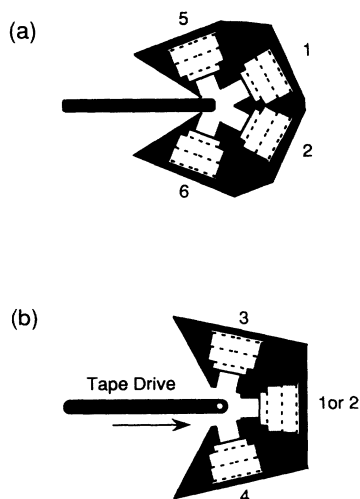


FIG. 2. Schematic diagram of the low-energy proton detector ball showing the relative location of the six telescopes and the tape drive. (a) A horizontal cross section. (b) A vertical cross section.

Cyclotron at Lawrence Berkeley Laboratory, while the target was  $\sim 2$  mg/cm<sup>2</sup> thick. The counting electronics were enabled only during the beam-off periods to eliminate neutron-induced background events. A representative two-dimensional plot showing one of the gas signals versus the silicon signal is given in Fig. 3(a), with the regions for betas, protons, and alpha particles indicated. The proton and alpha groups are (primarily) from the well-known delayed proton and alpha emitters  ${}^{25}\text{Si}$  [10] and  ${}^{20}\text{Na}$  [11], respectively, produced via the  ${}^{24}\text{Mg}({}^3\text{He}, 2n)$  and  ${}^{24}\text{Mg}({}^3\text{He}, \alpha p 2n)$  reactions.

The triple telescope technique is demonstrated in parts (b) and (c) of Fig. 3. In Fig. 3(b) the projected proton spectrum from the corresponding data of Fig. 3(a) is given. This projection is obtained by requiring that events lie within the proton region of only one of the  $\Delta E$ - $E$  plots. The spectrum in Fig. 3(c) shows the result when we require events to lie in the proton region of both  $\Delta E$ - $E$  plots (i.e., a triple coincidence event). In

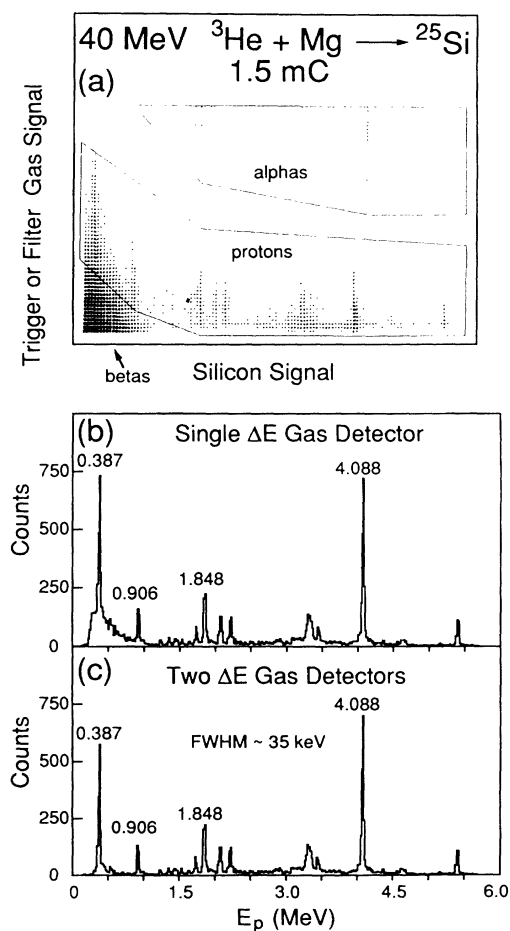


FIG. 3. Typical calibration data taken with one of the triple telescopes. (a) A two-dimensional plot showing one of the gas signals plotted versus the silicon signal. (b) The projected proton spectrum obtained by requiring that events lie within the proton region of only one of the  $\Delta E$ - $E$  plots. (c) The projected proton spectrum when events are required to lie within the proton region of both  $\Delta E$ - $E$  plots.

Fig. 3(c) the betas are completely suppressed in the region below  $\sim 1$  MeV, allowing even the weak proton peak at 534 keV [10] to be clearly resolved. It has been shown that this triple telescope design reduces the random beta rate which enters the low-energy proton region by a factor of  $> 10^6$ , allowing for the identification of protons on an event-by-event basis. It has also been demonstrated that gas- $\Delta E$ , Si- $E$  telescopes such as these provide a (identified) proton detection efficiency that is energy independent in the incident proton energy range from 250 to 6000 keV [9,10]. As indicated in the figure, proton resolutions of  $\sim 35$  keV [full width at half maximum (FWHM)] are obtained.

Proton calibrations for the telescopes were determined *in situ* utilizing the known  $^{25}\text{Si}$  delayed proton groups [10]. Only the Si-detector signals were used in the calibrations, with the gas signals utilized strictly for particle identification. For increasing proton energies above  $\sim 1.0$  MeV, the energy losses in the various telescope components are small (relative to the energy loss in the Si detector) and decrease very slowly. Thus neglecting these losses still results in a linear energy calibration. Although these energy losses become significant as the proton energy is decreased below 1.0 MeV, the  $^{25}\text{Si}$  lines provide reliable calibrations for proton energies down to  $\sim 390$  keV (i.e., to the lowest-energy  $^{25}\text{Si}$  proton line). At still lower proton energies, no known proton groups are available for calibration purposes. As our telescopes have proton thresholds of  $\sim 200$  keV, it was necessary to derive a dependable extrapolation technique.

A milked  $^{228}\text{Th}$  alpha source was utilized along with the semiempirical stopping power tables in Ref. [12] to measure directly the effective thicknesses of the various media a proton traverses in reaching a given Si detector. These include the region of helium between the collection point and the telescope, the entrance window of the telescope, the gas regions, and the Si-detector dead layer. Using the measured thicknesses of these components and the stopping power tables in Ref. [12], the energy losses prior to entering the active region of the Si detector were calculated for incident proton energies down to 100 keV. The energy measured in the Si detector is equal to the incident proton energy minus these prior losses (assuming linear Si-detector response). The thicknesses were varied within their respective uncertainties and the resulting predicted Si-detector energies fit to the observed groups of  $^{25}\text{Si}$  ( $E_p \geq 387$  keV) to obtain an optimum linear fit. This calibration was then used to find the energy lost in the Si detector by protons with incident energies less than 390 keV. Finally, by working backwards from the deduced energy deposited in the Si detector, the incident proton energies were determined using the optimum thicknesses of the various media between the Si-detector active volume and the collection point.

### III. EXPERIMENTAL RESULTS

We utilized the compound nuclear reaction  $^{24}\text{Mg}(p, n)$  at bombarding energies of 28.5 and 20.0 MeV to produce  $^{24}\text{Al}$  recoils. Pulsed proton beams with intensi-

ties of  $\sim 1 \mu\text{A}$  were employed, and again the counting electronics were only enabled during the beam-off cycle. The targets were  $1.9 \text{ mg/cm}^2$   $^{24}\text{Mg}$  (99.8% enriched). In the first experiment ( $E = 28.5$  MeV) a multiple-capillary, multiple-target system was used (see Ref. [13] for details). Five targets were placed in the helium-jet chamber, resulting in 11 of the internal capillaries being utilized to collect radioactivity. The 11 internal capillaries were then combined into a single transport capillary. While the production yield is increased with the multiple-capillary system, the transport time to the counting area is also increased significantly, as compared to a single-capillary system. In the second experiment ( $E = 20.0$  MeV) a single-capillary, single-target setup was used. The measured transit times were  $\sim 200$  and  $\sim 30$  ms for the multiple- and single-capillary systems, respectively [13]. Because of the relatively long half-life of  $^{24}\text{Al}$  (2.053 s) and the desire to compare the half-life of the proton continuum with the half-life of  $^{24}\text{Al}$  delayed alpha groups, the tape drive was stationary during both experiments.

In Fig. 4, the proton spectrum from a 4.7-mC bombardment at 28.5 MeV is shown. This spectrum represents the sum of proton events from three telescopes. In this experiment, the beam pulsing was set for a 500-ms bombardment followed by an 800-ms counting period. This beam energy is below threshold for the production of  $^{23}\text{Al}$ . A continuum of protons between  $\sim 300$  and 1100 keV is clearly evident. At this bombarding energy, the presence of  $^{20}\text{Na}$  alpha groups [11] precluded any attempt to cleanly identify the known alpha lines from  $^{24}\text{Al}$  [5].

In the second experiment, a proton beam energy of 20.0 MeV was used. The beam was pulsed such that the target was bombarded for 3 s, followed by a 4-s counting period. Although the statistical evaporation code ALICE [14] predicts the production cross section for  $^{24}\text{Al}$  to be reduced by a factor of  $\sim 5$ –10 at this energy as

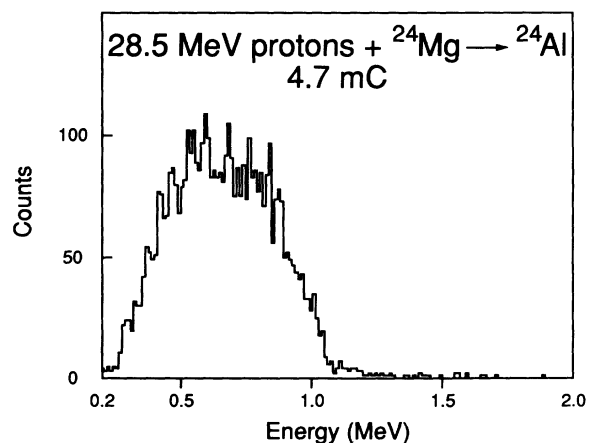


FIG. 4. Proton spectrum from the 28.5-MeV bombardment. Shown is the sum of proton events from three telescopes.

compared to the 28.5-MeV bombardment, the  $^{20}\text{Na}$  exit channel is closed. Hence the  $^{24}\text{Al}$  beta-delayed alpha groups were completely free of any background and one could compare their half-life with the low-energy proton events. A timing scalar was incremented throughout the phase when the counting electronics were enabled. Therefore, for each event, a time was recorded relative to the end of the target bombardment.

Figures 5 and 6 give the results from this 13-mC bombardment. In Fig. 5, a two-dimensional plot of gas- $\Delta E$  versus Si- $E$  is shown. Unlike the two-dimensional plot shown previously in Fig. 3(a), Fig. 5 is a “back-projected” two-dimensional spectrum. This trigger- $\Delta E$  versus Si- $E$  plot was generated by setting a loose two-dimensional gate in the “raw” filter- $\Delta E$  versus Si- $E$  space, which eliminated only the most intense beta region in the lower-left corner of the spectrum, and then back projecting these events into the trigger- $\Delta E$  versus Si- $E$  space. The proton gate shown in Fig. 5 was set using the strong proton lines from the  $^{25}\text{Si}$  calibration [compare Fig. 3(a)]. In Fig. 5, the known alpha lines from  $^{24}\text{Al}$  are clearly visible, while even with only this minimal gating the low-energy proton events are already emerging from the intense beta background. Figures 6(a) and 6(b) show the fully gated projected alpha and proton spectra, respectively, from the sum of two telescopes. Each of the four strongest known  $^{24}\text{Al}$  alpha groups [5] was observed. The two weaker  $^{24}\text{Al}$  alpha groups were not clearly evident because of low statistics and the alpha particle energy resolution of the telescopes. The low-energy proton continuum was also seen, although at a reduced intensity. Therefore this proton continuum can unambiguously be assigned to beta-delayed emission from  $^{24}\text{Al}$ . The insets in (a) and (b) of Fig. 6 present the half-life data, with statistical uncertainties, for each projection. The alpha half-life was determined using only the 1.982-MeV group to ensure that no (very small) contamination from any other alpha emitter (i.e.,  $^{24m}\text{Al}$ ; see below) was present. Because of continuous helium-jet transport, only times

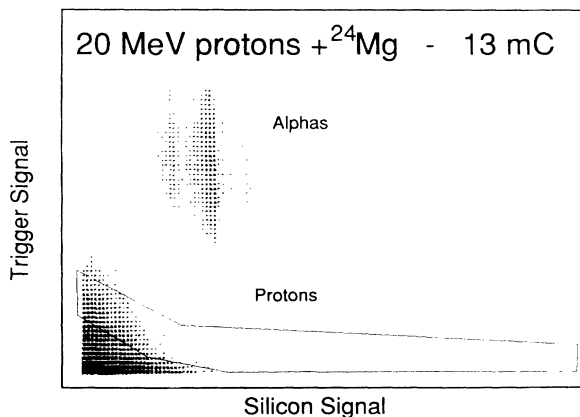


FIG. 5. Two-dimensional plot of one of the gas signals versus the silicon signal from the 20.0-MeV bombardment. The regions of betas, protons, and alpha particles are indicated.

much longer than the helium-jet transport time were used for half-life measurements.

There is a metastable state in  $^{24}\text{Al}$  at an excitation energy of 426 keV ( $^{24m}\text{Al}$ ) [15]. This state has an 82.5% gamma decay branch to the ground state of  $^{24}\text{Al}$  and a 17.5% beta-decay branch to  $^{24}\text{Mg}$  [5]. The known half-lives for the  $^{24}\text{Al}$  ground ( $^{24g}\text{Al}$ ) and metastable states are 2.053 s and 131 ms, respectively. Hence, for the multiple-capillary system used in the first experiment,  $\sim 70\%$  of the  $^{24m}\text{Al}$  entering the helium-jet system would have decayed before reaching the counting chamber. This fact, along with the relatively small beta-decay branch for  $^{24m}\text{Al}$ , implies that the proton continuum observed is due to beta-delayed proton emission from  $^{24g}\text{Al}$ . In the second experiment, the 4-s counting cycle favored  $^{24g}\text{Al}$  detection as compared with the shorter-lived  $^{24m}\text{Al}$ . In addition, an analysis which excluded any events occurring in the first 0.5 s of the counting period (which eliminates

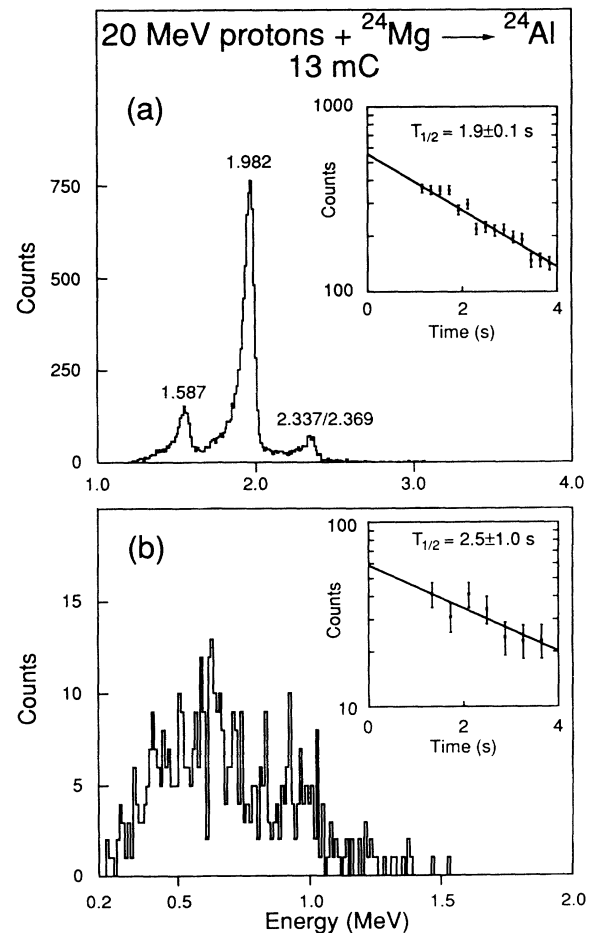


FIG. 6. Projected spectra from the 20.0-MeV bombardment. (a) The projected alpha spectrum from summing two telescopes. The inset shows the half-life data for the 1.982-MeV group. (b) The projected proton spectrum from summing two telescopes. The inset shows the proton half-life data.

well over 90% of a possible  $^{24m}\text{Al}$  component) resulted in a proton spectrum similar to that in Fig. 6(b), with a reduced intensity consistent with an  $\sim 2$ -s half-life source. Furthermore, none of the known delayed alpha groups [5] from  $^{24m}\text{Al}$  were observed in the second experiment. We therefore unambiguously assign the proton continuum to beta-delayed emission from  $^{24g}\text{Al}$ . (Any reference to  $^{24}\text{Al}$  will subsequently refer to  $^{24g}\text{Al}$ .)

The half-lives determined for the alpha and proton groups in the second experiment are consistent with each other and with the previously measured value for  $^{24}\text{Al}$  (2.053 s). This is a further confirmation of our assignment of the observed proton continuum. A gross half-life for the beta events was determined to be  $11.8 \pm 0.1$  s, consistent with an origin from a mixture of longer-lived beta emitters.

In Figs. 4 and 6(b), proton events with energies up to  $\sim 1500$  keV are apparent. While in principle these protons could originate via EC-delayed emission from  $^{24}\text{Al}$ , the ratio  $\Gamma_{\text{EC}}/\Gamma_{\beta+}$  is expected to be small. Furthermore, the ratio of the proton events at energies from  $\sim 1100$  to  $1500$  keV relative to the proton continuum between  $\sim 300$  and  $1100$  keV is not constant for the two bombarding energies. Electron-capture delayed alpha emission from  $^{24}\text{Al}$  has been observed. If, however, one takes the ratio of the EC-delayed alpha branch to the strongest positron-delayed branch [5] as an indication of the  $\Gamma_{\text{EC}}/\Gamma_{\beta+}$  ratio for  $^{24}\text{Al}$  and compares this to the peak in the observed proton continuum in Fig. 4, one would anticipate less than 0.1 counts per channel at proton energies greater than  $1100$  keV to be from EC-delayed proton emission from  $^{24}\text{Al}$ . Most likely, the proton events at energies above  $1100$  keV come from some (very small) contaminants in our helium-jet system. However, we cannot rule out that some (small) fraction of these events may be due to EC-delayed proton emission from  $^{24}\text{Al}$ .

#### IV. DISCUSSION

Figure 7 shows a proposed partial decay scheme for  $^{24}\text{Al}$ . States in  $^{24}\text{Mg}$  at excitation energies between  $11.69$  and  $12.86$  MeV are energetically open to positron-delayed proton emission, whereas emission of alpha particles following positron decay is energetically allowed for states with excitation energies between  $9.310$  and  $12.86$  MeV. Comparing the measured intensities of the proton continuum and the  $1.982$ -MeV alpha group, we determine a relative branching ratio of  $(4.7 \pm 0.2) \times 10^{-2}$ . If we then utilize the previously measured branching ratio for this  $^{24g}\text{Al}$  alpha group  $[(2.6 \pm 0.6) \times 10^{-4}$  [5]], we determine a branching ratio for beta-delayed proton emission of  $(1.2 \pm 0.3) \times 10^{-5}$ . This is in slight disagreement with the limit set in Ref. [6] of  $b_p \leq 8 \times 10^{-6}$ . However, the detectors utilized in the previous work were not as sensitive to low-energy protons as those used in the present experiments.

Based on an R-matrix formalism, the partial width for a particle decay channel can be written as

$$\Gamma_i = 2\gamma^2 P_\ell(E), \quad i = p, \alpha, \quad (1)$$

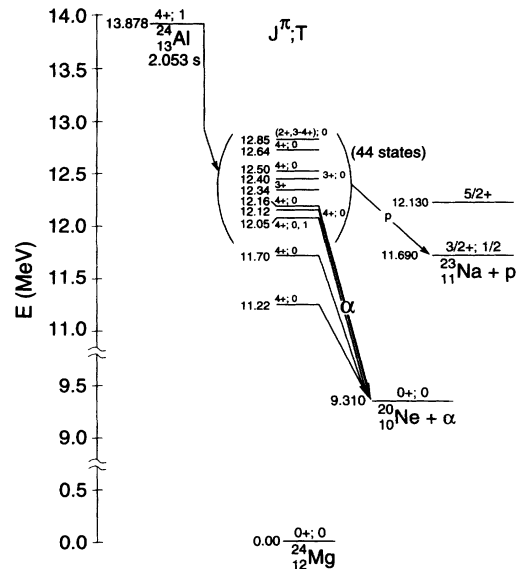


FIG. 7. Proposed partial decay scheme for  $^{24}\text{Al}$ .

where  $\gamma^2$  is the reduced width for the particle decay channel and  $P_\ell(E)$  is the penetrability for an alpha or proton with angular momentum  $\ell$  through the Coulomb and angular momentum barriers. The reduced width contains all of the nuclear wave function information and is completely determined by conditions in the interior of the nucleus. It can be written as

$$\gamma^2 = (\hbar^2/2\mu) S_{\ell j} | R_{n\ell j}(r_0) |^2 r_0. \quad (2)$$

Here  $S_{\ell j}$  is the spectroscopic factor,  $\mu$  is the reduced mass for the decay channel, and  $R_{n\ell j}$  is the radial part of the interior wave function, evaluated at the radius of the nuclear surface  $r_0$ . The square of this term represents the probability of finding a proton or alpha particle at the nuclear surface. The Bohr approximation [16] can be used for an orbital with small binding energy and is given as

$$r_0 | R_{n\ell j}(r_0) |^2 \approx 1.4/r_0^2. \quad (3)$$

The penetrability can be related to the regular and irregular Coulomb wave functions  $F_\ell$  and  $G_\ell$ , respectively, evaluated at the nuclear surface:

$$P_\ell(E) \propto \frac{1}{[F_\ell(r_0) + G_\ell(r_0)]}. \quad (4)$$

The above formalism has been utilized to calculate the penetrabilities for protons and alpha particles for  $\ell$  values between 0 and 4. In all cases we set the spectroscopic factor ( $S_{\ell j}$ ) equal to unity. The results of these calculations are presented in Fig. 8. To demonstrate the competition between the two decay modes, the horizontal axis represents the excitation energy in  $^{24}\text{Mg}$  (in MeV), rather than the proton or alpha-particle decay energies.

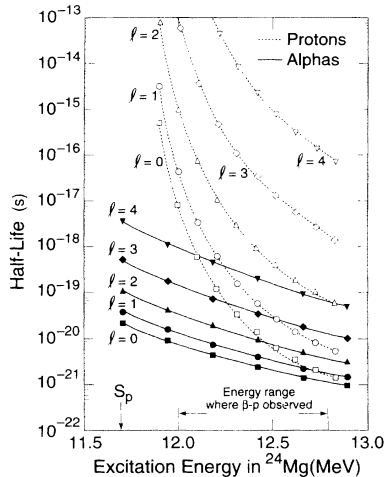


FIG. 8. Results of penetrability calculations for proton and alpha emission from excited states in  $^{24}\text{Mg}$ . Shown are the calculated half-lives for proton and alpha emission for  $0 \leq \ell \leq 4$ , plotted as a function of  $^{24}\text{Mg}$  excitation energy (see text).

Allowed beta decay from the  $^{24}\text{Al}$  ground state ( $J^\pi = 4^+$ ) populates states in  $^{24}\text{Mg}$  with  $J^\pi = 3^+, 4^+, \text{ or } 5^+$ . All of the (six) known delayed alpha groups from  $^{24}\text{Al}$  proceed through excited states in  $^{24}\text{Mg}$  with  $J^\pi = 4^+$ . They are then emitted via  $\ell = 4$  decays to the ground state of  $^{20}\text{Ne}$  ( $J^\pi = 0^+$ ). This is the only angular momentum which conserves both spin and parity for alpha decay to the ground state following allowed beta decay. Proton emission would be expected to proceed to the  $^{23}\text{Na}$  ground state ( $J^\pi = \frac{3}{2}^+$ ) with either  $\ell = 2$  or 4 following allowed beta decay of  $^{24}\text{Al}$ . (Proton decay to the ground state of  $^{23}\text{Na}$  rather than to excited states is strongly favored due to the sharp increase in partial proton half-life with decreasing decay energy.)

Referring to Fig. 8, it can be seen that  $\ell = 2$  proton

emission is favored over  $\ell = 4$  proton decay by  $\sim 3$  orders of magnitude. Hence the quasicontinuum of protons we observe should be due to states in  $^{24}\text{Mg}$  with  $J^\pi = 3^+, 4^+$  (assuming allowed beta decay). As indicated in Fig. 7, there are over 40 states known in the region of  $^{24}\text{Mg}$  excitation energies accessible to positron-delayed proton emission [17]. As illustrated by the nondiscrete nature of the protons observed, it appears that a significant number of these states are populated in the beta decay of  $^{24}\text{Al}$  and subsequently decay by proton emission. If one further compares  $\ell = 2$  proton decay with  $\ell = 4$  alpha decay in Fig. 8, their respective partial half-lives are similar only after  $\sim 13.0$  MeV in excitation energy is reached. However, proton competition with alpha decay is already observed at  $\sim 12.0$  MeV in excitation energy. This could readily be due to the fact that alpha-particle preformation factors and other nuclear structure effects were neglected in these calculations.

## V. CONCLUSIONS

Utilizing the  $^{24}\text{Mg}(p, n)$  reaction, helium-jet transport techniques, and our new low-energy proton detector ball, beta-delayed proton decay from  $^{24}\text{Al}$  has been observed for the first time. The protons form a quasicontinuum from  $\sim 300$  to 1100 keV. By comparing the proton yield with a previously observed delayed alpha group, we determine a beta-delayed proton decay branching ratio of  $(1.2 \pm 0.3) \times 10^{-5}$ . This beta-delayed proton branch of  $^{24}\text{Al}$  makes it the lightest known member of the  $A = 4n, T_z = -1$  series to exhibit both beta-delayed proton and alpha decay. Most probably, the protons arise via  $\ell = 2$  emission from  $J^\pi = 3^+$  and  $4^+$  excited states in  $^{24}\text{Mg}$  to the ground state of  $^{23}\text{Na}$ .

This work was supported by the Director, Office of Energy Research, Office of High Energy and Nuclear Physics, Division of Nuclear Physics, of the U.S. Department of Energy under Contract No. DE-AC03-76SF00098.

- [1] B. Jonson and G. Nyman, in *Handbook of Nuclear Decay Modes* (CRC, Boca Raton, FL, in press).
- [2] J.C. Hardy and E. Hagberg, in *Particle Emission from Nuclei*, edited by D.N. Poenaru and M.S. Ivascu (CRC, Boca Raton, FL, 1989), Vol. 3, p. 99.
- [3] J.E. Steigerwalt, J.W. Sunier, and J.R. Richardson, Nucl. Phys. **A137**, 585 (1969).
- [4] D.F. Torgerson, N.S. Oakey, and R.D. MacFarlane, Nucl. Phys. **A178**, 69 (1971).
- [5] J. Honkanen, M. Kortelahti, J. Äystö, K. Eskola, and A. Hautojärvi, Phys. Scr. **19**, 239 (1979).
- [6] J. Honkanen, J. Äystö, and K. Eskola, Phys. Scr. **34**, 608 (1986).
- [7] J.C. Batchelder, D.M. Moltz, T.J. Ognibene, M.W. Rowe, and J. Cerny, Phys. Rev. C **47**, 2038 (1993).
- [8] D.M. Moltz, J.C. Batchelder, T.J. Ognibene, M.W. Rowe, R.J. Tighe, and J. Cerny (in preparation).
- [9] D.M. Moltz, J.D. Robertson, J.C. Batchelder, and J. Cerny, Nucl. Instrum. Methods Phys. Res., Sect. A. (in press).
- [10] J.D. Robertson, D.M. Moltz, T.F. Lang, J.E. Reiff, J. Cerny, and B.H. Wildenthal, Phys. Rev. C **47**, 1455 (1993).
- [11] E.T.H. Clifford *et al.*, Phys. Rev. Lett. **50**, 23 (1983).
- [12] *Stopping Powers and Ranges for Protons and Alpha Particles*, International Commission on Radiation Units and Measures, Report 49 (1993), M.J. Berger, Chairman of the Report Committee.
- [13] D.M. Moltz, J.M. Wouters, J. Äystö, M.D. Cable, R.F. Parry, R.D. Von Dincklage, and J. Cerny, Nucl. Instrum. Methods **172**, 519 (1980).
- [14] M. Blann and J. Bisplinghoff, Lawrence Livermore National Laboratory Report No. UCID-19614, 1982 (unpublished).
- [15] A.J. Armini, J.W. Sunier, R.M. Polichar, and J.R. Richardson, Phys. Lett. **21**, 335 (1966).
- [16] A. Bohr and B. Mottelson, *Nuclear Structure* (Benjamin, New York, 1969), Vol. 1, p. 326.
- [17] P.M. Endt, Nucl. Phys. **A521**, 1 (1990).

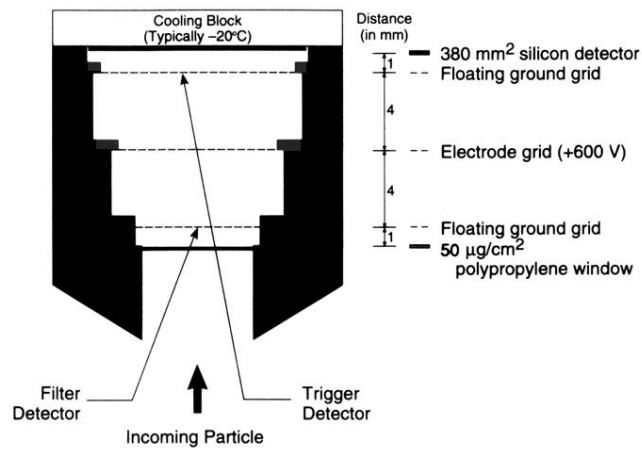


FIG. 1. Cross sectional view of one of the low-energy gas- $\Delta E$ , gas- $\Delta E$ , Si- $E$  triple telescopes.

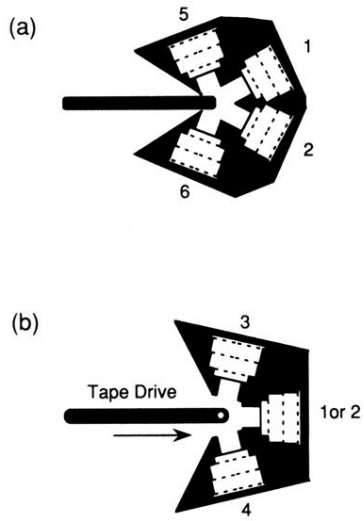


FIG. 2. Schematic diagram of the low-energy proton detector ball showing the relative location of the six telescopes and the tape drive. (a) A horizontal cross section. (b) A vertical cross section.